APPLIED MICROBIAL AND CELL PHYSIOLOGY

The cytotoxicity and anticancer mechanisms of alterporriol L, a marine bianthraquinone, against MCF-7 human breast cancer cells

Caihuan Huang · Hua Jin · Bing Song · Xun Zhu · Hongxia Zhao · Jiye Cai · Yongjun Lu · Bin Chen · Yongcheng Lin

Abstract Alterporriol L, a new bianthraquinone derivative, was isolated from a marine fungus *Alternaria* sp. ZJ9-6B. The cytotoxic activity and anticancer mechanisms of alterporriol L towards breast cancer cells lines were detected using MTT assay, immunofluorescence, and flow cytometry. Simultaneously, the changes in morphological properties of cells were detected before and after treatment with alterporriol L by atomic force microscope (AFM) at a nanometer scale. MTT assay showed that alterporriol L could effectively inhibit the growth and proliferation, and there was a dose-dependent manner of cell death. Moreover, the alterporriol L could induce cancer cell apoptosis or necrosis. Furthermore, the reactive oxygen species, mitochondrial membrane potential, and cytosolic free calcium level were changed after treatment with alterporriol L, suggesting that alterporriol L played vital roles in breast cancer cells through destroying the mitochondrial. And all these alterations are in accord with changes of morphology detected by AFM, which suggested that the AFM is a useful tool to detect the morphological changes of the cancer cells.

Keywords Marine bianthraquinone · Breast cancer · Apoptosis · Atomic force microscopy

Caihuan Huang, Hua Jin, and Bing Song contributed equally to this work.

C. Huang · B. Chen · Y. Lin (✉)
School of Chemistry and Chemical Engineering,
Sun Yat-sen University,
Guangzhou 510275, China
e-mail: ceslyc@mail.sysu.edu.cn

C. Huang · X. Zhu · Y. Lu · B. Chen · Y. Lin
Guangdong Province Key Laboratory of Functional Molecules
in Oceanic Microorganism (Sun Yat-sen University),
Bureau of Education of Guangdong,
Guangzhou, China

C. Huang
School of Science and Engineering, Jinan University,
Guangzhou 510632, China
e-mail: thamy@jnu.edu.cn

H. Jin · J. Cai
Department of Chemistry, Jinan University,
Guangzhou 510632, China

B. Song
The Institute for Tissue Transplantation and Immunology,
Jinan University,
Guangzhou 510632, China

H. Zhao
Faculty of Chemical Engineering and Light Industry,
Guangdong University of Technology,
Guangzhou 510090, China

Introduction

Over the decades, marine microorganisms are increasingly attracting attention as they produce a wide variety of secondary metabolites that are structurally unique and pharmacologically active (Bhadury et al. 2006; Kharwar et al. 2011). To date, with the isolation of thousands of bioactive metabolites, marine microorganisms have proved to be a rich and promising source of novel antibacterial and anticancer natural products (Mayer et al. 2007; Mayer and Gustafson 2008; Rateb and Ebel 2011). Chemical structures of these natural products include polyketides, peptides, terpenes, steroids, and so on. Moreover, the fact that metabolites can be produced in bulk through manufacturing culture systems makes drug discovery based on marine microbiology a pharmaceutically promising approach (Demain 2000).

Bianthraquinone, one kind of polyketide metabolite, had been isolated from marine fungi and plants, which showed cytotoxicity against different types of cancer cell lines, e.g., KB, HeLa, and L5178Y cells (Phuwapraisirisan et al. 2009; Debbab et al. 2009). In our ongoing research on bioactive natural products, a new marine bianthraquinone named alterporriol L [(6S*,7R*,8R*)-4,4′,6,7,7′,8-hexahydroxy-1,1′-dimethoxy-6′,7-dimethyl-5,6,7,8-tetrahydro-[2,2′-bianthracene]-9,9′,10,10′-tetraone)] was isolated from a mangrove endophytic fungus Alternaria sp. ZJ9-6B. This compound showed an interesting coupling position at C-2-C-2′ and exhibited cytotoxic activity towards breast cancer cells lines (Huang et al. 2011). Interestingly, its substructure was similar with epiadriamycin, an anticancer drug used widely in the clinic. We used breast cancer cell lines MCF-7 cells and MDA-MB-435 cells as a model to investigate the anticancer activity of alterporriol L. Simultaneously, MTT assay, immunofluorescence, and flow cytometry were used to analyze its underlying molecular mechanisms. And, the changes in morphological and biomechanical properties of cells before and after treatment with alterporriol L were also detected by atomic force microscopy (AFM) at nanometer scale.

With the development and application of AFM, the AFM-based technology has been extensively used in biochemical and pharmaceutical fields. The high-resolution imaging mode of AFM allows it to obtain the images of the cell morphology (Binning et al. 1986; Iscru et al. 2008), and membrane ultrastructure (Muller 2008; Wang et al. 2009) at nanometer or molecular level. Comparing with the traditional microscopy, AFM has some obvious advantages. As we know, light microscopy is useful for identifying cells, as well as for determining their general shape, but the resolution is submitted to by light diffraction limitation (Lange et al. 2001), and the best resolution is lower than half wavelength of detection light (>0.3 μm). Electron microscopy techniques can provide high-resolution images of cells, but this method requires vacuum conditions (Tai and Tang 2001), which means that it cannot detect the live cells in aqueous solutions. And on the other side, the sample preparations require chemical fixation, negative stain, cryofixation, dehydration, embedding, sectioning, freeze-fracture or freeze-etch, conductive coating, etc. So, with all these treatments, the delicate structures of sample will be disturbed. In comparison, AFM allows sample observation in nearly physiological state at room temperature or in aqueous solution.

Materials and methods

Chemicals rhodamin 123, Fluo-3 AM, Annexin V-FITC/PI apoptosis detection kit, 3-[4,5-dimethylthiazol-2-yl]-2,5 diphenyl tetrazolium bromide (MTT), 2′,7′-dichlorofluorescein

diacetate (DCFH-DA), 4,6-diamidino-2-phenylIndole (DAPI), and fluorescein isothiocyanate (FITC)–phalloidin were purchased from Beyotime Institute of Biotechnology, China. All reagents used in the experiments were of analytical grade.

Endophytic fungi and cancer cell lines

The fungus ZJ9-6B was obtained from the fruit of a mangrove tree Aegiceras corniculatum collected on the coast of Zhanjiang, in Guangdong province, China, in 2008. It was tentatively named Alternaria sp. ZJ9-6B and deposited in the Marine Culture Collection Center of China with accession number MCCC 3J00047. It was identified according to a molecular biological protocol by DNA amplification and sequencing of the ITS region with an ITS sequence GenBank number FJ 037770. Human breast cancer cell lines MCF-7 and MDA-MB-435 were purchased from ATCC (USA).

Fermentation of endophytic fungi and preparation of alterporriol L

The fungus was incubated in potato dextrose broth (PDB) medium (dextrose 20 gL^{-1} and crude sea salt 3 gL^{-1} in potato infusion) at 28 ± 1°C for 30 days under stationary conditions. The mycelium was dried and soaked in the methanol after separated from the cultures (200 L) with filtration. And then, the methanol extract was subjected to a combination of column chromatography on silica gel, Sephadex LH-20, and C_{18} reversed phase silica gel to isolate and purify the alterporriol L. The structure of alterporriol L (Fig. 1) was determined mainly by one—and two—dimensional NMR spectroscopy, MS data analysis. The compound was dissolved in dimethylsulfoxide (DMSO) to make a stock solution at a concentration of 1 mM which was then diluted to appropriate concentrations with culture medium before each experiment. The final concentration of DMSO did not exceed 0.5% in any experiment.

Cell culture

Human breast cancer cell lines MCF-7 and MDA-MB-435 were supplemented with 5% fetal bovine serum (Hyclone, Logan, UT, USA), 2 mM L^{-1} glutamine, 100 μg mL^{-1} streptomycin, and 100 IU mL^{-1} penicillin (Invitrogen) at
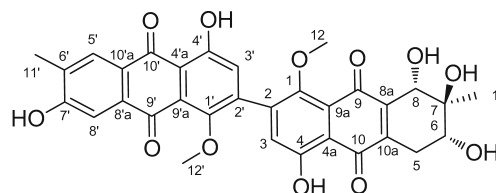

Fig. 1 Structure of alterporriol L isolated from Alternaria sp. ZJ9-6B

37°C in a humidified atmosphere of 5% CO_2. Two MCF-7 cells and MDA-MB-435 experimental groups were designed: (a) control cells and (b) cells treated with different concentrations (final concentration of 10, 20, and 40 μM) of alterporriol L.

MTT assay

Cell viability was assessed by the MTT assay. MCF-7 and MDA-MB-435 cells (1×10^4 cells/well) were treated with different concentrations of alterporriol L in 96-well culture plates for 48 h. During the last 4 h, cells were reacted with MTT at 37°C for colorimetric MTT-based cytotoxicity assay.

Determination of apoptosis rate

An Annexin V-FITC/PI apoptosis detection kit was used to detect early apoptotic activity. After treating with alterporriol L, the detection method was according to the manufacturer's instructions. Briefly, the cells were washed with cold PBS and suspended in 500 μL Annexin V binding buffer. After stained with 5 μL FITC-labeled Annexin V and 5 μL PI, and incubated for 30 min at room temperature in the dark, the samples were immediately measured by a flow cytometer (BD FACSAria™).

Measurement of reactive oxygen species production

Moreover, the intracellular reactive oxygen species (ROS) production was determined using DCFH-DA. DCFH-DA is a nonfluorescent probe, but it can be deacetylated by esterases to form nonfluorescent 2′,7′-dichlorofluorescin (DCFH) when it passively diffuses into cells. DCFH can react with ROS to form the fluorescent product 2′,7′-dichlorofluorescein (DCF) in the presence of ROS. The MCF-7 cells before and after treatments of alterporriol L were incubated with 10 μM of DCFH-DA for 20 min at 37°C. Then, the fluorescence intensity was measured at 485 nm for excitation and 530 nm for emission with a flow cytometer to elucidate the production of ROS.

Measurements of mitochondrial membrane potential and cytosolic free calcium level

To detect the changes in mitochondrial membrane potential (MMP) and cytosolic free calcium levels, the MCF-7 cells treated with alterporriol L at designated concentrations were incubated with rhodamin 123 and Fluo-3 AM away from the light for 30 min at room temperature separately. The cells were collected and washed twice with PBS. The resulting fluorescence was analyzed by the flow cytometer.

Immunofluorescent staining

The morphology of apoptosis and cytoskeleton were evaluated by staining with DAPI and FITC–phalloidin separately. The cells with or without alterporriol L treatments were fixed with 4% paraformaldehyde for 30 min and incubated with 50 μM of DAPI for 15 min and 1 μM FITC–phalloidin for 60 min in the dark at room temperature separately. After that, the cells were washed with PBS. Then, the nuclear morphology and organization of cytoskeleton were imaged by a Carl Zeiss LCM 510 Meta Duo Scan laser scanning confocal microscope.

Single-cell AFM measurement

A tapping mode AFM (Autoprobe CP Research, Veeco, USA) was used to obtain topographic images of cells. To remove any organic contaminates, the silicon Nitride tips (UL20B, Park Scientific Instruments) used in all AFM measurements were irradiated with ultraviolet in air for 15 min prior to use. An optical microscope was used to help select the desired cells. The curvature radius of the tips is less than 10 nm, and the thickness, width, and length of the cantilevers are 3.5, 30, and 115 μm, respectively, with a force constant of 0.01 N/m and an oscillation frequency of 255 kHz. Single-cell imaging was performed on more than five cells in each group. All images were only analyzed by the instrument-equipped software IP 2.1 to gain information of the topography. The Ra is the average roughness in analytical area.

Statistical analysis was performed with Student's t test, and statistical significance was assessed at the $p < 0.05$ level.

Results

Alterporriol L was red power, dissolvable in acetone, methanol, and dimethylsulfoxide, with the maximum absorption wavelength locating at about 225.50 nm. It was elucidated as a bianthraquinone with an anthraquinone unit and a tetrahydroanthraquinone unit using spectral analysis (Fig. 1). Its optical rotation was $[\alpha]_D^{25} = +30$ ($c = 1.0$, MeOH) which indicated the possibility of an asymmetric center and/or axial chirality.

Analysis of cells viability and apoptosis induced by alterporriol L

Cytotoxicity of alterporriol L in human breast cancer cell lines MCF-7 (lower metastasizing cells) and MDA-MB-435 (higher metastasizing cells) cell lines were determined by MTT assay (Fig. 2a). After treatment for 48 h, alterporriol L exhibited a dose-dependent markedly inhibited growth on

Fig. 2 a Cytotoxicity of cells treated with different concentrations of alterporriol L for 48 h detected by MTT assay. b The apoptotic rate of cells after alterporriol L treatment measured by annexin V-FITC-based flow cytometry
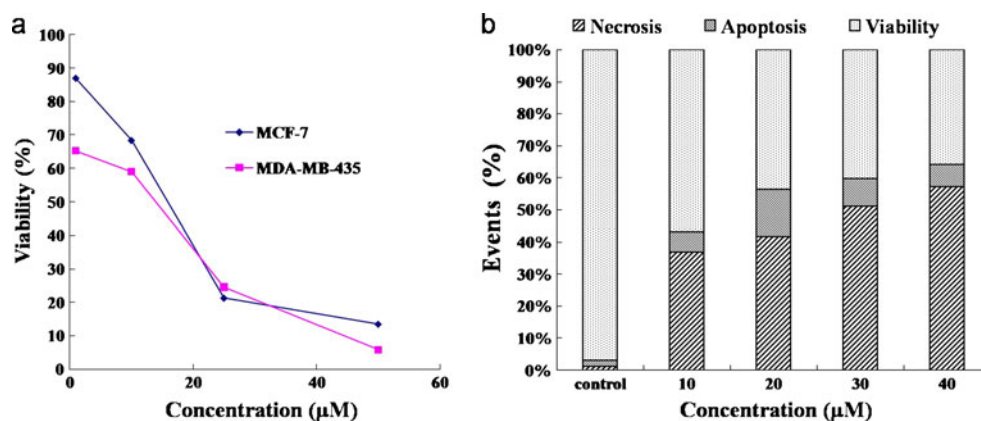
both cells lines, compared with that of control cells. The IC_{50} values were 20.04 μM for MCF-7 and 13.11 μM for MDA-MB-435, respectively. And, over 86% cells can be killed when the concentration of alterporriol L increased to 50 μM.

To assess the extent and mode of cell death of MCF-7, annexin V-FITC/PI staining was carried out, which evaluated phosphatidylserine turnover from the inner to the outer lipid layer of the plasma membrane, an event typically associated with apoptosis. Statistical data were extracted from the dot plots using WinMDI software, which indicated the percentages of those with red fluorescent labels (necrotic cells), green labels (apoptotic cells), and unstained cells (viable cells) were analyzed. The data (Fig. 2b) showed that over 64% cells can be killed (the sum of necrotic and apoptotic cells) by 40 μM of alterporriol L. Figure 2b demonstrated that the death rate of the cells was 43.20%, 56.36%, 59.71%, and 64.06%, when treated with alterporriol L at concentrations of 10, 20, 30, and 40 μM, respectively. This indicated that there was a dose-dependent relationship of death rate (the sum of necrosis and apoptosis) of MCF-7 cells. Moreover, alterporriol L mainly induced the necrosis of MCF-7 cells, and only a portion of cells was caused to apoptosis. When treated with 20 μM of alterporriol L, there appears the max apoptotic rate (14.77%).

Taken together, alterporriol L could effectively inhibit the growth and proliferation of MCF-7, and there was a dose-dependent manner of cell death. Particularly, the alterporriol L mainly induced the cell necrosis, but only a portion of cells were in the state of apoptosis.

Changes in ROS production of cells induced by alterporriol L

Previous studies have shown that ROS, by-products of aerobic metabolism, plays vital roles in intracellular signaling cascades (Orrenius 1993; Denning et al. 2002; Lin et al. 2004). Mitochondria were one of the major sources of intracellular ROS whose overproduction can trigger stress pathway that ultimately leads to cell apoptosis (Ortiz-Sánchez et al. 2009).

Interestingly, mitochondria were both the source and target of ROS. Ye et al. (2010) and Saito et al. (2006) reported that ROS induced mitochondrial dysfunction, which contributed to cell death. Moreover, Gao et al. (2005) and Satya et al. (2011) reported that the mechanism of most chemotherapeutic agents kill tumor cells was generation of ROS. Thus, we investigated the changes in production of ROS of cells before and after being treated with different concentrations (10 to 40 μM) of alterporriol L staining with DCFH-DA.

Figure 3a, b, c showed the date detected by flow cytometer, and the mean fluorescence intensity (MFI) indicated the ROS production. There was a significant increase of ROS production in the cells treated with alterporriol L, which is indicated by the increase in MFI of DCFH-DA (shown in Fig. 3c). Results of flow cytometry with these cells implicated a major role of oxidative stress in an induction of apoptotic and necrotic change in MCF-7 cells. Taking our results together, we have demonstrated that alterporriol L triggered oxidative stress in MCF-7 cells.

Changes in mitochondrial membrane potential

Characterization of the toxicity-induced MMP loss plays vital roles in screening drug candidates. With mitochondrial damage or loss of MMP, rhodamin 123 could be released from the mitochondria and produce fluorescence, which is indicated by a decrease of MFI. As shown in Fig. 3d, e, f, there is a remarkable decrease of MFI in MCF-7 cells compared with that of control group, which indicated that the rapid drop in MMP induced by alterporriol L. Owing to the destruction of the outer membrane induced by alterporriol L, the permeability transition pore was opened or the voltage-dependent anion channels in the mitochondrial outer membrane were closed, and these changes would lead to the remarkable loss of MMP (Andrew et al. 2002). Previous studies have reported that MMP loss could cause cytochrome c release and caspase activation (Jared et al. 2000; Douglas and Guido 2004), which play important roles in the induction of cell death (necrosis or apoptosis).
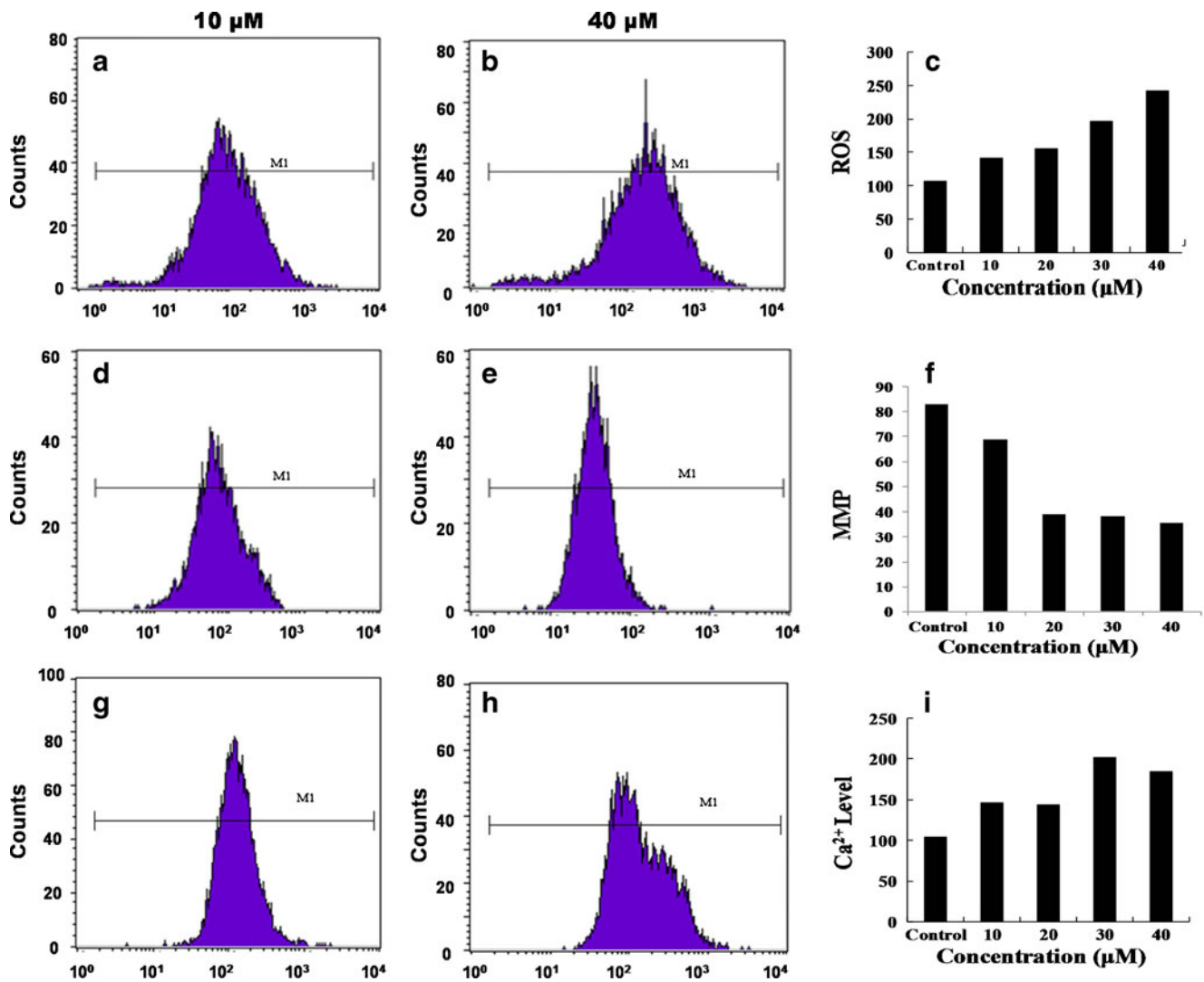
Fig. 3 Flow cytometric analysis of ROS (**a–c**), MMP (**d–f**), and intracellular Ca^{2+} level (**g–i**) in MCF-7 cells treated with serial concentrations of alterporriol L. The resulting MFI was the indicator of ROS, MMP, or intracellular Ca^{2+} levels. The significant reduction in MMP and increase in ROS and intracellular Ca^{2+} levels indicated that alterporriol L treatments could induce MCF-7 cell apoptosis or necrosis at a large extent

Therefore, alterporriol L induced loss of MMP should play key roles in the necrosis or apoptosis of MCF-7 cells.

Intercellular free Ca^{2+} detection

Intracellular calcium was a highly versatile signaling molecule regulating various vital cell functions, such as cell growth, proliferation, signal transduction, and so on (Berridge et al. 2000). There was a significant literature that suggested that the central function of Ca^{2+} is the regulation of programmed cell death (Orrenius et al. 2003). So, we measured the intensity of intracellular fluo-3 fluorescence, an indicator of Ca^{2+} level, in MCF-7 cells before and after treatment with alterporriol L. As shown in Fig. 3g, h, i, there is a significant increase in intracellular calcium of cells treated with alterporriol L, comparing with that of

control cells. Diverse abnormal cellular processes, even apoptosis, can be triggered by the influx of Ca^{2+} released from the internal stores or from the environment. Cell signaling can be activated by a temporary increase in cytoplasmic calcium level through the opening of calcium channels in the plasma membrane or the endoplasmic reticulum (Duchen 2000). The rise in cytoplasmic Ca^{2+} level induced by alterporriol L might be largely associated with the collapse of membrane integrity (Fig. 5) which could promote the opening of Ca^{2+} channels in cell membrane and the consequent influx of Ca^{2+}.

Immunofluorescence

The control cells showed a shuttle- or polygon-like shape (Figs. 4, 5, and 6), but the cells became retracted and
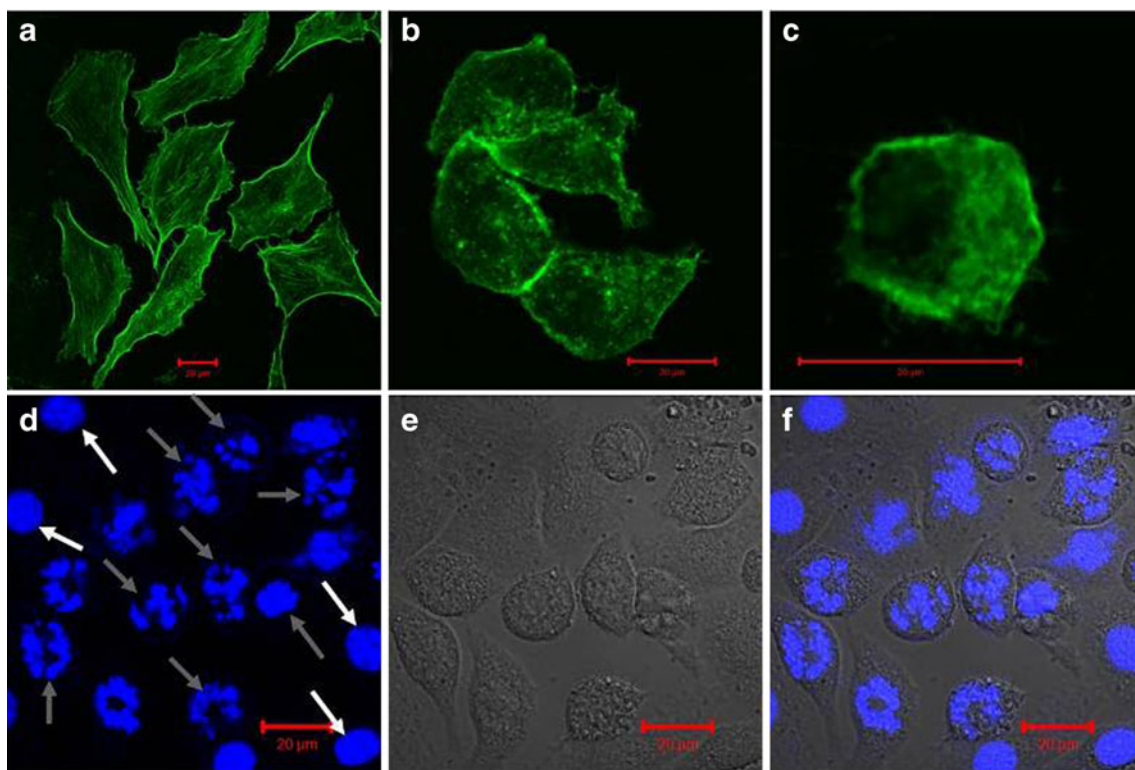
Fig. 4 Immunofluorescent data of MCF-7 cells treated with different concentrations of alterporriol L. **a**–**c** Reorganization of cytoskeleton in cells stained with FITC–phalloidin. **d**–**f** Nuclei of normal and apoptotic cells stained with DAPI. The fluorescence image, the phase image, and the merged one are shown in **d**, **e**, and **f**, respectively. In **d**, the *white arrows* indicated the nuclei of normal cells and the *gray arrows* showed the nuclei of apoptotic cells. After treatment with alterporriol L, the cells shrunk and became rounded (**b**, **c**), the cytoskeleton networks disappeared (**b**, **c**), and the nuclei staining (**d**) represented fragmented morphology of nuclear bodies, which indicated the apoptosis induction by alterporriol L

contractive after alterporriol L treatment (Fig. 5). Previous reports had provided evidence that cytoskeleton alterations could induce apoptosis as well as necrosis in a variety of model (Shimizu et al. 1996; Grzanka et al. 2003; Melanie et al. 2008; Olivia et al. 2008). Thus, it is very important to investigate whether alterporriol L had effects on arrangement of cytoskeleton. Figure 4 showed the reorganization of F-actins of MCF-7 cells stained with FITC–phalloidin. The assembly of actins in control cells represented regular mesh networks (Fig. 4a), while after alterporriol L treatments, the cells shrunk and became rounded, the cytoskeletal networks disappeared, the actin microfilaments disrupted and appeared in condensed aggregates, and even the cell integrity was damaged (Fig. 4b).

To further investigate whether alterporriol L induced the apoptosis of MCF-7 cells, the assay was performed using DAPI staining. When DAPI bind to natural double-stranded DNAs, the fluorescence is strongly enhanced and the morphology of the nuclei can be clearly visualized, based on which the apoptotic cells can be identified. Figure 4d, e, f revealed the typical nuclei morphology (Escobar et al. 2008) in the DAPI-stained MCF-7 cells treated with 20 μM alterporriol L. There were intact, plump nuclei in control

cells (white arrows in Fig. 4d). But the nuclei of apoptotic cells represented the changes involved in the segmentation of nucleus and the condensed chromatin gathering at the periphery of the nuclear membrane (gray arrows in Fig. 4d). Taken together, the data indicated that alterporriol L could significantly inhibit proliferation and induce apoptosis of MCF-7 cells.

AFM analysis

Changes in cell morphology

AFM, a nondestructive surface imaging tool, can obtain images of cell surface at the molecular level which can provide us important details on the architecture of cell membranes. Here, the tapping mode AFM was used for cell imaging and to observe various changes in surface morphology and ultrastructure of MCF-7 cells treated with different concentration of alterporriol L.

Figure 5 showed AFM images of MCF-7 cells. Control cells had a regular ovoid or spindle shape, and the cell surface was relatively smooth and intact (Fig. 6a, b, c). And there were pseudopodium connecting each other to ex-
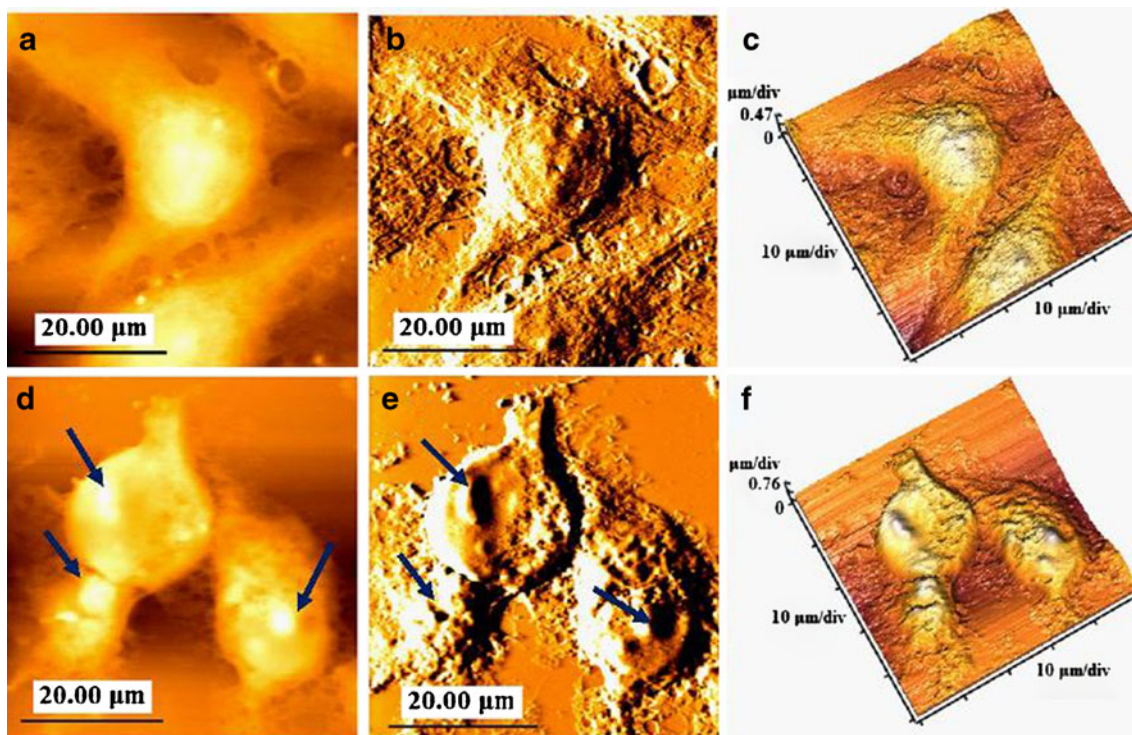
Fig. 5 AFM topographic data of MCF-7 cells. **a–c** Control MCF-7 cells. **d–f** MCF-7 cells treated with 40 μM alterporriol L for 48 h. **a** and **d** are the topography mode, **b** and **e** are the error signal mode of **a** and **d**, and **c** and **f** are the 3-D mode of **a** and **d**, respectively. Scanning area, **a–f** 50×50 μm²

change material and transfer information between the cells. Figure 6d indicated the MCF-7 cells treated with 40 μM alterporriol L for 48 h, the cells became rounded and the number of the pseudopodium decreased significantly. Besides, the morphological changes, such as blebbing, pores, and apoptotic bodies, that appeared over the cell
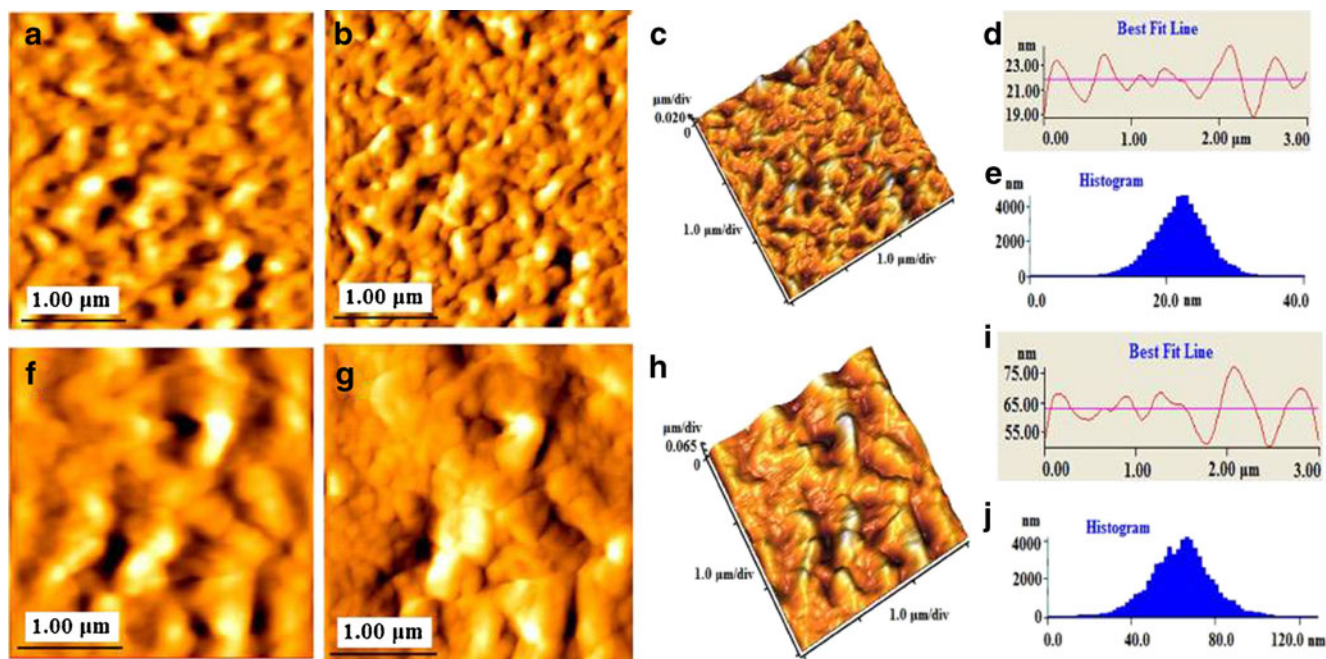

Fig. 6 AFM ultrastructural data of control MCF-7 cells (**a–e**) and MCF-7cells treated with 40 μM alterporriol L (**f–h**). **d** and **i** height profiles, **e** and **j** histograms of the particle size extracted from images **a** and **f**, respectively. **a** and **f** are the topography mode, **b** and **g** are the error signal mode of **a** and **f**, and **c** and **h** are the 3-D mode of **a** and **f**, respectively. Scanning area, **a–f** 3×3 μm²

surface (Fig. 5d, e, f), were similar to the characteristics of apoptosis or necrosis.

Meanwhile, AFM can reveal the alternations of cell surface ultrastructure at nanometer scale. Figure 6 showed the ultrastructural data of MCF-7 cells. The cell membrane architecture of control cells (Fig. 6) was homogeneous and represented granular morphology with the surface particles of around 22 nm. Figure 6d showed the cell surface architecture of MCF-7 cells with alterporriol L treatment. Furthermore, the cytoskeleton structure of control cell presented regular networks of F-actins (shown in Fig. 4), while after alterporriol L treatment, the cytoskeleton networks disappeared and presented a gathered state (shown in Fig. 4b, c). The nanoparticles on cell membrane were not of uniform size and the surface particles size increased to 62 nm (Fig. 6h, i, j) from 22 nm of control cells (Fig. 6c, d, e). Taken together, all these morphological data revealed that there were dose-dependent changes in morphological data of cells treated with alterporriol L. And at the concentration of 20 μM of alterporriol L, it mainly induced cell apoptosis. Especially, the alternations in ultrastructure of cytoskeleton and membrane surface might result from the altered chemical composition of the out membrane. This provided more detailed information for the understanding of the membrane toxicity induced by alterporriol L.

Discussion

The MTT assay indicated that alterporriol L inhibited the proliferation and growth of breast cancer cells in a dose-dependent manner. Additionally, alterporriol L could induce necrosis as well as apoptosis of cells, which was indicated by an annexin V-FITC/PI apoptosis detection kit. Moreover, the alternations in the cytoskeleton and nuclei morphology also showed cell apoptosis or necrosis induced by alterporriol L.

Oxidative stress due to accumulation of ROS has been implicated in triggering cell death (Pierre and Guido 2006; Oh and Lim 2006; Rongbin et al. 2011). ROS led to the free radical attack of membrane phospholipids and loss of MMP, which induced the intermembrane proteins (such as cytochrome c) release out of the mitochondria, opening of mitochondrial permeability transition pore, and Ca^{2+} efflux from the cytoplasm (Paul et al. 2004; Shih et al. 2004). After treating with alterporriol L, the increased level of ROS suggested that alterporriol L triggered the generation of oxidative stress. Besides, the rapid increase of cytosolic free Ca^{2+} and the collapse of MMP detected by flow cytometry further confirmed that the mitochondrial apoptotic pathway was one of the main anticancer mechanisms of alterporriol L.

To better understand the results, we investigated the changes in cell topography, membrane surface ultrastructure

with AFM. AFM morphological data indicated that cell surface changed from a homogeneous to a heterogenous morphology, and there were shrinkage, blebbing, and pores that appeared. Furthermore, the ultrastructure of control cell presented regular networks of F-actins (shown in Fig. 4), while after alterporriol L treatment, the cytoskeleton networks disappeared and presented a gathered state (shown in Fig. 4b, c). And the particles size of cell surface also increased to 62 nm (Fig. 6h, i, j) from 22 nm of control cells (Fig. 6c, d, e). This suggested that the altered chemical composition of the outer membrane or reduction in the number of microvilli induced by alterporriol L. With the application of AFM, the subtle changes in the structural of cancer cell were detected at the nanometer scale before and after treatment with alterporriol L, which contributed to throwing light on the structure–function relationship of cell surfaces and to the better understanding of the interaction between cells and drugs during the chemotherapy.

In summary, we first isolated alterporriol L from the endophytic fungus ZJ9-6B. This method could produce quantities of alterporriol L by fermentation process and ensure a sustainable application for further pre-clinical and clinical researches. Moreover, the cytotoxicity experiments also indicated that alterporriol L could effectively inhibit the proliferation and growth of breast cancer cell line MCF-7 and MDA-MB-435 cells. The anticancer mechanisms and morphological alterations were also detected. The experiments performed in this study could provide protocols to develop and screen new drug leads for other researchers.

References

Andrew P, Halestrap GPM, Samantha JC (2002) The permeability transition pore complex: another view. Biochimie 84:153–166
Berridge MJ, Lipp P, Bootman MD (2000) The versatility and universality of calcium signalling. Nat Rev Mol Cell Biol 1:11–21
Bhadury P, Mohammad BT, Wright PC (2006) The current status of natural products from marine fungi and their potential as anti-infective agents. J Ind Microbiol Biotechnol 33:325–337
Binning G, Quate CF, Gerber C (1986) Atomic force microscope. Phys Rev Lett 56:930–933
Debbab A, Aly AH, Edrada-Ebel R, Wray V, Müller WEG, Totzke F, Zirrgiebel U, Schächtele C, Kubbutat MHG, Lin WH, Mosaddak M, Hakiki A, Proksch P, Ebel R (2009) Bioactive metabolites from the endophytic fungus Stemphylium globuliferum isolated from Mentha pulegium. J Nat Prod 72:626–631
Demain AL (2000) Small bugs, big business: the economic power of the microbe. Biotechnol Adv 18:499–514

Denning TL, Takaishi H, Crowe SE, Boldogh I, Jevnikar A, Ernst PB (2002) Oxidative stress induces the expression of Fas and Fas ligand and apoptosis in murine intestinal epithelial cell. Free Radical Biol Med 33:1641–1650

Douglas RG, Guido K (2004) The pathophysiology of mitochondrial cell death. Science 305:626–629

Duchen MR (2000) Mitochondria and Ca^{2+} in cell physiology and pathophysiology. Cell Calcium 28(6):339–348

Escobar ML, Echeverría RO, Vázquez-Nin GH (2008) Combined apoptosis and autophagy, the process that eliminates the oocytes of atretic follicles in immature rats. Apoptosis 13:1253–1266

Gao J, Liu X, Rigas B (2005) Nitric oxide-donating aspirin induces apoptosis in human colon cancer cells through induction of oxidative stress. Proc Natl Acad Sci USA 102:17207–17212

Grzanka A, Grzanka D, Orlikowska M (2003) Cytoskeletal reorganization during process of apoptosis induced by cytostatic drugs in K-562 and HL-60 leukemia cell lines. Biochem Pharmacol 66:1611–1617

Huang CH, Pan JH, Yu M, Huang HB, Zhu X, Lu YJ, She ZG, Lin YC (2011) Three bianthraquinone derivatives from the mangrove endophytic fungus *Alternaria* sp. ZJ9-6B from the South China Sea. Mar Drugs 9(5):832–843

Iscru DF, Anghelina M, Agarwal S, Agarwal G (2008) Changes in surface topologies of chondrocytes subjected to mechanical forces: an AFM analysis. J Struct Biol 162(3):397–403

Jared LS, Philip WS, Gillian H, Elizabeth CL, Hung-Hai K, Micheal PM (2000) Changes in mitochondrial membrane potential during staurosporine-induced apoptosis in Jurkat cells. FEBS letter 475:267–272

Kharwar RN, Mishra A, Gond SK, Stierle A, Stierleb D (2011) Anticancer compounds derived from fungal endophytes: their importance and future challenges. Nat Prod Rep. doi:10.1039/c1np00008j

Lange F, Cambi A, Huijbens A, Bakker B, Rensen W, Garcia-Parajo M, Hulst N, Figdor C (2001) Cell biology beyond the diffraction limit: near-field scanning optical microscopy. J Cell Sci 114:4153–4160

Lin Y, Choksi S, Shen HM, Yang QF, Hur GM, Kim YS (2004) Tumor necrosis factor-induced nonapoptotic cell death requires receptor-interacting protein-mediated cellular reactive oxygen species accumulation. J Biol Chem 279:10822–10828

Mayer AM, Gustafson KR (2008) Marine pharmacology in 2005–2006: antitumour and cytotoxic compounds. Eur J Cancer 44:2357–2387

Mayer AM, Rodriguez AD, Berlinck RG, Hamann MT (2007) Marine pharmacology in 2003–2004: marine compounds with anthelmintic, antibacterial, anticoagulant, antidiabetic, antifungal, anti-inflammatory, antimalarial, antiplatelet, antiprotozoal, antituberculosis, and antiviral activities; affecting the cardiovascular, immune and nervous systems and other miscellaneous mechanisms of action. Comp Biochem Physiol C Toxicol Pharmacol 145(4):553–581

Melanie H, Amanda MGV, Pieter S, Geerten NA, Rene M, Johan G (2008) Rho-kinase-dependent F-actin rearrangement in involved in the inhibition of PI3-kinase/Akt during ischemia-reperfusion-induced endothelial cell apoptosis. Apoptosis 13(3):404–412

Muller DJ (2008) AFM: a nano tool in membrane biology. Biochemistry 47(31):7986–7998

Oh SH, Lim SC (2006) A rapid and transient ROS generation by cadmium triggers apoptosis via caspase-dependent pathway in HepG2 cells and this is inhibited through N-acetylcysteine-mediated catalase upregulation. Toxicol Appl Pharm 212:212–223

Olivia NT, Jocelyne H, Jacqueline B (2008) Cytoskeleton and apoptosis. Biochem Pharmacol 76:11–18

Orrenius S (1993) Mechanisms of oxidative cell damage. In: Poli G, Albano E, Dianzani MU (eds) Free radicals: from basic science to medicine. Birkhauser Verlag, Basel, pp 47–64

Orrenius S, Zhivotovsky B, Nicotera P (2003) Regulation of cell death: the calcium-apoptosis link. Nat Rev Mol Cell Biol 4:552–565

Ortiz-Sánchez E, Daniels TR, Helguera G, Martinez-Maza O, Bonavida B, Penichet ML (2009) Enhanced cytotoxicity of an anti-transferrin receptor IgG3-avidin fusion protein in combination with gambogic acid against human malignant hematopoietic cells: functional relevance of iron, the receptor, and reactive oxygen species. Leukemia 23:59–70

Paul SB, Yisang Y, James LR, Anders MW, Shey-Shing S (2004) Calcium, ATP, and ROS: a mitochondrial love-hate triangle. Am J Physiol Cell Physiol 287(4):817–833

Phuwapraisirisan P, Rangsan J, Siripong P, Tip-pyang S (2009) New antitumour fungal metabolites from *Alternaria* Porri. Nat Prod Res 23:1063–1071

Pierre G, Guido K (2006) Cell death by necrosis: towards a molecular definition. Trends Biochem Sci 32(1):37–43

Rateb ME, Ebel R (2011) Secondary metabolites of fungi from marine habitats. Nat Prod Rep 28:290–344

Rongbin Z, Amir SY, Philippe M, Jürg T (2011) A role for mitochondria in NLRP3 inflammasome activation. Nature 469:221–226

Saito Y, Nishio K, Ogawa Y, Kimata J, Kinumi T, Yoshida Y, Noguchi N, Niki E (2006) Turning point in apoptosis/necrosis induced by hydrogen peroxide. Free Radic Res 40:619–630

Satya SP, Indira J, Gayathri C, Sandeep S, Anand S, Gregory RJT, Stephen S (2011) GT-094, a NO-NSAID, inhibits colon cancer cell growth by activation of a reactive oxygen species-microRNA-27a: ZBTB10-specificity protein pathway. Mol Cancer Res 9(2):195–205

Shih CM, Ko WC, Wu JS, Wei YH, Wang LF, Chang EE, Lo TY, Cheng HH, Chen CT (2004) Mediating of caspase-independent apoptosis by cadmium through the mitochondria-ROS pathway in MRC-5 fibroblasts. J Cell Biochem 91:384–397

Shimizu S, Eguchi Y, Kamiike W (1996) Induction of apoptosis as well as necrosis by hypoxia and predominant prevention of apoptosis by Bcl-2 and Bcl-X$_L$. Cancer Res 56:2161–2166

Tai SSW, Tang XM (2001) Manipulating biological samples for environmental scanning electron microscopy observation. Scanning 23(4):267–272

Wang J, Wan Z, Liu W, Li L, Ren L, Wang X, Sun P, Ren L, Zhao H, Tu Q, Zhang Z, Song N, Zhang L (2009) Atomic force microscope study of tumor cell membranes following treatment with anti-cancer drugs. Biosens Bioelectron 25(4):721–727

Ye JS, Li J, Yu YM, Wei Q, Deng WF, Yu LX (2010) L-carnitine attenuates oxidant injury in HK-2 cells via ROS-mitochondria pathway. Regul Pept 161:58–66